Journal of Environmental Management 393 (2025) 127287

Contents lists available at ScienceDirect

Journal of Environmental Management

journal homepage: www.elsevier.com/locate/jenvman

Research article

Metal(loid) removal from highly metal rich acid mine waters using natural schwertmannite

Carlos R. Cánovas [a,*], Maira Castellanos [a], Rafael Pérez-López [a], Ricardo Millán-Becerro [b], Alberto Molinero-García [a], Manuel Olías [a], José Miguel Nieto [a], María Dolores Basallote [c]

[a] Department of Earth Sciences & Research Center on Natural Resources, Health and the Environment. University of Huelva, Campus "El Carmen", E-21071, Huelva, Spain
[b] Department of Soil Science and Agricultural Chemistry, University of Granada, Avda. Fuente Nueva s/n, E-18071, Granada, Spain
[c] Department of Ecology and Coastal Management, Institute of Marine Sciences of Andalusia (ICMAN-CSIC), E-11510, Puerto Real, Spain

ARTICLE INFO

Keywords:
Circular economy
Acid mine drainage
Sorption processes
Schwertmannite

ABSTRACT

This study evaluates the potential of natural schwertmannite for treating highly acidic and metal-rich effluents (pH 2.0) containing high concentrations of Fe (6664 mg/L), Al (910 mg/L), Zn (794 mg/L), Cu (196 mg/L), As (12.5 mg/L), and Pb (0.17 mg/L) through batch and column experiments. In batch experiments, schwertmannite interaction with acidic waters led to increased dissolved concentrations of sulfate (19 %), Fe (14 %), and Al (6 %), especially at a 1:10 solid-to-liquid ratio, likely due to schwertmannite dissolution. Other elements such as Cr, Cu, Ni, Cd, Se, U, Th, and REEs followed the same trend, with Cr later showing 22 % removal and Zn ranging from 1.3 % to 5.5 %. Most notably, As and Pb were effectively removed, with efficiencies of 82–88 % and 90–93 %, respectively. The column experiment also demonstrated high As and Pb removal rates (63–99 % and 74–92 %, respectively). After stabilization, most elements showed slight concentration increases (1–8 %) at the end of the experiment, while Cr, Ga, Se, Cd, U, and Y exhibited net removal rates of 10–49 %, 7–38 %, 3–24 %, 8–11 %, 1–15 %, and 3–20 %, respectively. Fe solubility in the column experiment was controlled by jarosite precipitation and schwertmannite dissolution. The mobility of other elements was influenced by sorption and/or coprecipitation onto these minerals, depending on their speciation. Negatively charged species were preferentially removed by sorption onto the positively charged schwertmannite surface, while others coprecipitated with newly formed jarosite. Maximum sorption values reached 97–181 mg/g for As and 0.8–0.9 mg/g for Pb. The adsorption capacity of natural schwertmannite was notable compared to synthetic schwertmannite, nanostructured cerium-manganese oxide, biochars, Fe-Mn polymers, and low-cost materials like eggshells and tea waste. Given its effectiveness, schwertmannite from AMD systems could serve as a natural filter at treatment plant inlets.

1. Introduction

Acid mine drainage (AMD) is a significant environmental concern worldwide associated to the oxidation of sulfides and characterized by the release of acidic and metal-laden waters into surrounding ecosystems (Akcil and Koldas, 2006). This pollutant process has been widely reported in literature. Johnson and Hallberg (2005) estimated in 1989 around 19,300 km of rivers and 720 km^2 of lakes and reservoirs strongly affected by AMD worldwide. Concomitant to mining activities, significant examples of AMD affection have been reported in USA (Ziemkiewicz et al., 2003), Australia (Naidu et al., 2019), China (e.g., Cai, 2015; He et al., 2018) or Spain (Nieto et al., 2013). AMD constitutes a severe risk to aquatic life and may have far-reaching ecological consequences as well as pose a threat to human health (Hudson-Edwards, 2016; Chen et al., 2022); thus, the adoption of effective and sustainable treatment methods to avoid or mitigate these potential impacts is of paramount importance. In this context, active treatments involve a high energy consumption and the continuous addition of chemical reagents, while passive treatments use renewal energy sources (e.g., gravity, energy of microbial metabolism, photosynthesis or energy released from geochemical reactions; Akcil and Koldas, 2006). Moreover, passive treatments require minimal maintenance compared to active treatments. Consequently, active treatments are typically employed in operational mines where large volumes of water must be treated before

* Corresponding author.
E-mail address: carlos.ruiz@dgeo.uhu.es (C.R. Cánovas).

https://doi.org/10.1016/j.jenvman.2025.127287
Received 19 June 2025; Received in revised form 26 July 2025; Accepted 7 September 2025
Available online 11 September 2025

discharge, while passive treatments are generally more suitable for abandoned mines or during post-closure remediation efforts (Johnson and Hallberg, 2005). While passive treatments are generally eco-friendlier and more economical than active ones, the production of chemical reagents such as calcite and dolomite involves substantial costs and environmental impacts. Thus, a more sustainable and budget-friendly solution could be implemented.

In this sense, schwertmannite is a Fe oxyhydroxysulfate with a variable chemical composition ($Fe_8O_8(OH)_{8-x}(SO_4)_x \cdot nH_2O$, where $1 < x < 1.75$), and widely present in acidic sulfate and iron rich aqueous systems (Bigham et al., 1996). The existence of structural defects reduces the coherent domain size of schwertmannite to just a few nanometers, resulting in a nanomineral with a large surface area and high sorption capacity, which makes this mineral an excellent scavenger of pollutants in aqueous systems (e.g., Antelo et al., 2012; Schoepfer and Burton, 2021; Carrero et al., 2022). The accumulation of this mineral in the different components of passive treatment plants (i.e., lagoons, settling ponds, channels and so on) requires its removal and disposal in safe conditions. For example, after 840 days of functioning, around 6.5 tons of Fe, mainly precipitated as schwertmannite, were accumulated in the natural Fe(II) oxidation lagoon at the entrance of the Mina Esperanza passive treatment plant based on disperse alkaline substrate technology (Orden et al., 2021). The recycling of these Fe-rich wastes as sorbent would improve the environmental footprint of this technology, saving costs associated to their transport and disposal while improving the performance of the water treatment. While schwertmannite has shown promise in removing contaminants from wastewater, many studies have not fully addressed its long-term stability, regeneration capacity, or leaching behavior under environmental conditions. Moreover, few have explored large-scale or field applications using naturally occurring schwertmannite, which offers the dual benefit of treating wastewaters with a waste. In addition, these Fe minerals usually host significant concentrations of impurities which could be released during the treatment. Hence, the suitability of using schwertmannite wastes generated in AMD environments should be previously evaluated.

For these reasons, the main goals proposed in this study are: i) to investigate the sorption capacity of naturally precipitated schwertmannite to treat highly-acid and metal/loid-rich mine waters and ii) to determine the potential release of impurities from these Fe-rich wastes during the treatment. The ubiquitous nature of this mineral in different Earth surface systems (e.g., AMD, acid sulfate soils, marshlands and so on) makes the results of this study being highly applicable to other natural systems worldwide.

2. Methods

2.1. Material sampling and characterization

Schwertmannite samples (2 kg) were collected from the Natural Fe Oxidation Lagoon (NFOL) of Mina Esperanza, where Fe(II) is naturally oxidized and schwertmannite spontaneously precipitates and accumulated in the bottom (Orden et al., 2021). Prior to experimentation, this material was chemically characterized after total acid digestion with aqua regia at the R + D Services of the University of Huelva using ICP-AES (Jobin Yvon Ultima 2) for major elements and ICP-MS (Agilent 7700) for trace elements. The detection limits were 0.25 mg/L for S; 0.1 mg/L for Na, Fe, K, Mg, and Si; 0.02 mg/L for Al and Ca; and 2 μg/L for the trace elements. The analytical precision was assessed by triplicate analyses of selected samples with values below 5 % in all cases. Blanks were also analyzed in each analysis sequence, with all elements below the detection limit. The analytical accuracy was evaluated by the analysis of reference materials (NIST-1640) and home-made solutions, with differences below 6 % between these and the referenced concentrations. Solid samples were also mineralogically characterized before starting and after ending the experiments. The mineralogical composition of solid samples was determined by X-ray diffraction (XRD) at the R + D Services of the University of Huelva using a Bruker D8 Advanced X-ray diffractometer employing Cu K-alpha radiation. The selected settings were 40 kV, 30 mA, a scan range of 3–65° 2Θ, 0.02° 2Θ step size, and 2.4 s counting time per step. In addition, samples were examined under a JEOL JSM-IT500HR Field Emission Scanning Electron Microscope coupled with Oxford XMax 150 Energy Dispersive System (FESEM-EDS) at the R + D Services of the University of Huelva.

In order to perform the experiments, around 25 L of acidic and metal-rich AMD was collected from Poderosa Mine (Huelva, Spain), one of the most pollutant sources in the upper section of the Odiel River, which exhibits a high variability. For example, the dissolved Fe pollutant load released through the mine gallery ranges from ~100 to 200 kg/day of Fe during base flow to almost 2200 kg/day during the flow peak (Cánovas et al., 2018). To determine the chemical composition of the water, samples were filtered (through 0.22 μm), acidified to pH < 1 and refrigerated until analysis by ICP-AES and ICP-MS. Different physico-chemical parameters such as temperature, pH, electrical conductivity (EC) and oxidation-reduction potential (ORP) were measured using a CRISON MM40+ equipment. A three-point calibration was performed for both EC and pH (147, 1413 μS/cm and 12.88 mS/cm, and 4.01, 7.00 and 9.21, respectively), while the ORP was controlled using two reference solutions (240 and 470 mV). The ORP values were corrected to obtain the potential referred to the hydrogen electrode (Nordstrom and Wilde, 1998) and finally pE values required for modelling.

2.2. Batch and column experiments

Two distinct methods were used to evaluate the effectiveness of schwertmannite as a remediation agent for highly acidic, metal-laden AMD waters. To determine the optimal amount of schwertmannite, batch experiments in 50 ml polyethylene tubes were conducted with two different solid-to-liquid ratios (S:L) (1:10, and 1:20). Kinetic effects were also assessed by testing different reaction intervals (5 min, 15 min, 30 min, 2 h, 4 h, 6 h, 12 h, 24 h, 48 h, and 96 h). During each experiment, the samples were continuously stirred, and at each specified reaction time, samples were extracted, centrifuged, filtered through 0.22 μm cellulose nitrate filters, and then acidified with ultrapure HNO_3 before analysis. Physical and chemical parameters (pH, ORP, electrical conductivity, and temperature) were measured in each sample following this procedure. The adsorption capacity at equilibrium Q_e (mg/g) during batch experiments was calculated using the following equation:

$$Qe = \frac{(Co - Ce)\ V}{m}$$

where C_0 (mg/L) and C_e (mg/L) are the initial and final concentration of elements, respectively, V(L) is the AMD solution volume and m(g) is adsorbent mass.

Column experiments were also conducted to evaluate the dynamic adsorption behavior of the material under continuous flow conditions. These tests provide insight into the practical applicability of the adsorbent, which cannot be fully assessed in batch experiments alone. The setup was composed of an initial 5L tank to store AMD water, which was connected to the top part of a column through a peristaltic pump set to a constant flow rate of 0.3 mL/min. The column, constructed from HDPE with a diameter of 6 cm and a length of 40 cm, was filled with a mixture of schwertmannite and wood shavings (20 % Schw and 80 % wood shavings) to ensure permeability. Inside the column, the flow is downward by gravity. At the bottom of each column, a 3 cm layer of silica sand was added to improve drainage. The column was linked to a 445 cm^3 settling pond to collect treated water and allow for the flocculation and sedimentation of precipitated minerals. The column experiments ran for 25 days, with samples collected at varying intervals—daily during the first week, then every 2–3 days afterwards. Each sample followed the same procedures as in batch experiments, including

measuring physico-chemical parameters, filtration, acidification, and analysis. At the end of the experiment, the column was dismantled, and solid samples were collected and processed for mineralogical analysis.

2.3. Geochemical modelling and statistical analysis

Metal speciation and saturation indices of the waters were determined using the PHREEQC code v3.73 (Parkhurst and Appelo, 2013). The Minteq v4 database was expanded to include thermodynamic data for schwertmannite (Bigham et al., 1996) along with additional minerals such as melanterite ($Fe(SO_4)•7H_2O$), copiapite ($Fe_5(SO_4)_6(OH)_2•20H_2O$), and coquimbite ($Fe_2(SO_4)_3•9H_2O$), sourced from other databases available within the PHREEQC code.

3. Results

3.1. Characterization of starting materials

Schwertmannite used in the experiments is mainly composed of Fe (47.6 %) and S (5.5 %), which accounts for a Fe/SO_4 molar ratio of 4.95, within the common range observed for schwertmannite (from 8 to 4.5; Bigham et al., 1996). In addition, the schwertmannite used in the experiments hosted significant concentrations of As (1405 mg/kg) and Al (867 mg/kg) (Table 1). The incorporation of Al into the structure of Fe-oxide/hydroxisulfate minerals has been widely reported, generally by the replacement of Fe in octahedral coordination by Al and by adsorption (e.g., Sánchez-España et al., 2016; Carrero et al., 2022). Under acidic conditions, the surface of schwertmannite is positively charged leading to a strong affinity for oxyanions such as As, Cr, V or Mo (e.g., Antelo et al., 2012). This would explain the high concentrations of Al and As in the schwertmannite used. In fact, around 560 and 10.3 kg of Al and As, respectively, were accumulated in the schwertmannite precipitated in the Mina Esperanza NFOL (Orden et al., 2021). Minor concentrations of other elements commonly found as oxyanions (274 mg/kg of V, 6.4 mg/kg of Sb, 0.5 mg/kg of Se) and metals (112 mg/kg of Cu, 80 mg/kg of Zn, 11 mg/kg of Mn, 8.8 mg/kg of Cr, 6.2 mg/kg of Ge or <1 mg/kg of REE and Y) were also found in schwertmannite (Table 1). While direct measurements of specific surface area (SSA), pore size distribution (PSD), and zeta potential (ZP) were not performed on our field-collected schwertmannite, previous studies reported SSA values of up to 330 m^2/g, PSD of 3 nm for micropores and 30 nm for micropores, and ZP values close to 7.2 in acid mine drainage settings (Schoepfer and Burton, 2021).

On the other hand, AMD samples used for column experiments exhibited a very low pH value (2.05) and high EC (14.3 mS/cm), and dissolved concentrations of major components (Table 2) such as sulfate (20814 mg/L), Fe (6664 mg/L), Al (910 mg/L), Zn (794 mg/L), Ca (211 mg/L), Cu (196 mg/L), Mn (80 mg/L) or Si (62 mg/L). According to the Ficklin diagram, these waters can be classified as high acid-extreme metal waters. This diagram is commonly used to categorize AMD waters according to their pH and base metal concentrations (Ficklin et al., 1992). It is also striking the high concentrations found for some trace elements such as As (12.5 mg/L), Co (11.2 mg/L) or Ni (2.6 mg/L). In turn, other trace elements exhibited concentrations below 1 mg/L (Table 2), highlighting the concentrations observed for V (837 μg/L), Cr (637 μg/L), and some rare earth elements such as Ce (357 μg/L), Y (270 μg/L) or Nd (238 μg/L).

Table 1
Chemical composition (in mg/kg, except for Fe and S in $\%_{wt}$) of the schwertmannite samples used in the batch and column experiments.

Schwertmannite composition			
mg/kg			
Fe	47.6 %	**Sb**	6.4
S	5.5 %	**Ge**	6.2
As	1405	**Ga**	3.7
Al	867	**Ce**	0.86
Ca	541	**Nd**	0.76
Mg	439	**Y**	0.51
P	377	**Se**	0.48
V	274	**La**	0.28
K	174	**Sc**	0.23
Cu	112	**U**	<0.1
Zn	80	**Th**	<0.1
Na	74	**Tl**	<0.1
Pb	31	**Co**	<0.1
Mn	11	**Cd**	<0.1
Cr	8.8	**Ni**	<0.1

Table 2
Main physico-chemical parameters (i.e., pH, EC and ORP), major and trace elements of AMD used for the experiments.

AMD input			
mg/L		μg/L	
pH	2.04	**V**	837
CE (mS/cm)	14.3	**Cr**	637
ORP (mV)	250	**Ce**	357
Sulfate	20,814	**Y**	270
Fe	6664	**Nd**	238
Al	910	**Pb**	169
Zn	794	**La**	96
Ca	211	**Ge**	74
Cu	196	**Ga**	73
Mn	80	**Se**	68
Si	62	**U**	50
As	12.5	**Sc**	38
Co	11.2	**Er**	31
K	7.1	**Yb**	26
Phosphate	5.8	**Th**	11.3
Ni	2.6	**Sb**	5.0
Cd	1.5	**Tl**	5.0

3.2. Batch experiments

The contact of AMD with schwertmannite caused a slight increase in pH values (ratio 1:10 and 1:20), from 2.04 to 2.21, although this maximum value was achieved before with the S:L ratio 1:20 (12h; Fig. 1), compared to the ratio 1:10 (48h). Afterwards, pH values decreased slightly to the end of the experiment, with a final value of 2.18 at 96 h (Fig. 1). This initial increase in pH values coincided with a moderate increase in electrical conductivity (EC) values; from 14.3 to 15.5 mS/cm, reaching the maximum values at the beginning of the solid-water interaction (t = 5 min). During the experiment, ORP values increased from the initial value of 250 mV to maximum values of 557 mV (ratio 1:10 at 2h) and 401 mV (ratio 1:20 at 48h), indicating the predominance of oxidation reactions.

The interaction of the acidic waters with schwertmannite led to the increase in Fe, sulfate and Al, especially for the ratio 1:10 with increases of up to 19 % and 14 % with respect initial concentrations of sulfate and Fe at 48 h, respectively (Fig. 1). The increase of Al for the ratio 1:10 was more limited, not exceeding a 6 % of increase regarding initial concentrations. These increases could be related to the dissolution of schwertmannite during the interaction of the acidic waters with this mineral. These processes seem also to occur, although to a lesser extent, in the 1:20 ratio experiment (Fig. 1). Other elements also seem to be affected by dissolution or desorption processes (Fig. 1 and Fig. S1). For example, Cr and Cu concentrations increased up to 18 % and 3.8 %, respectively at 2 h (ratio 1:10; Fig. 1), although in the case of Cr, a progressive depletion is observed thereafter, with a maximum removal of 22 % at the end of the experiment. For the ratio 1:20, a net slight depletion of both elements is observed during the experiment. A similar depletion pattern is observed for Zn, with removal values ranging from 1.3 to 5.5 % for both ratios (Fig. 1). Other elements such as Ni, Cd, Se, U, Th and REE were in turn released from the solid during the experiment

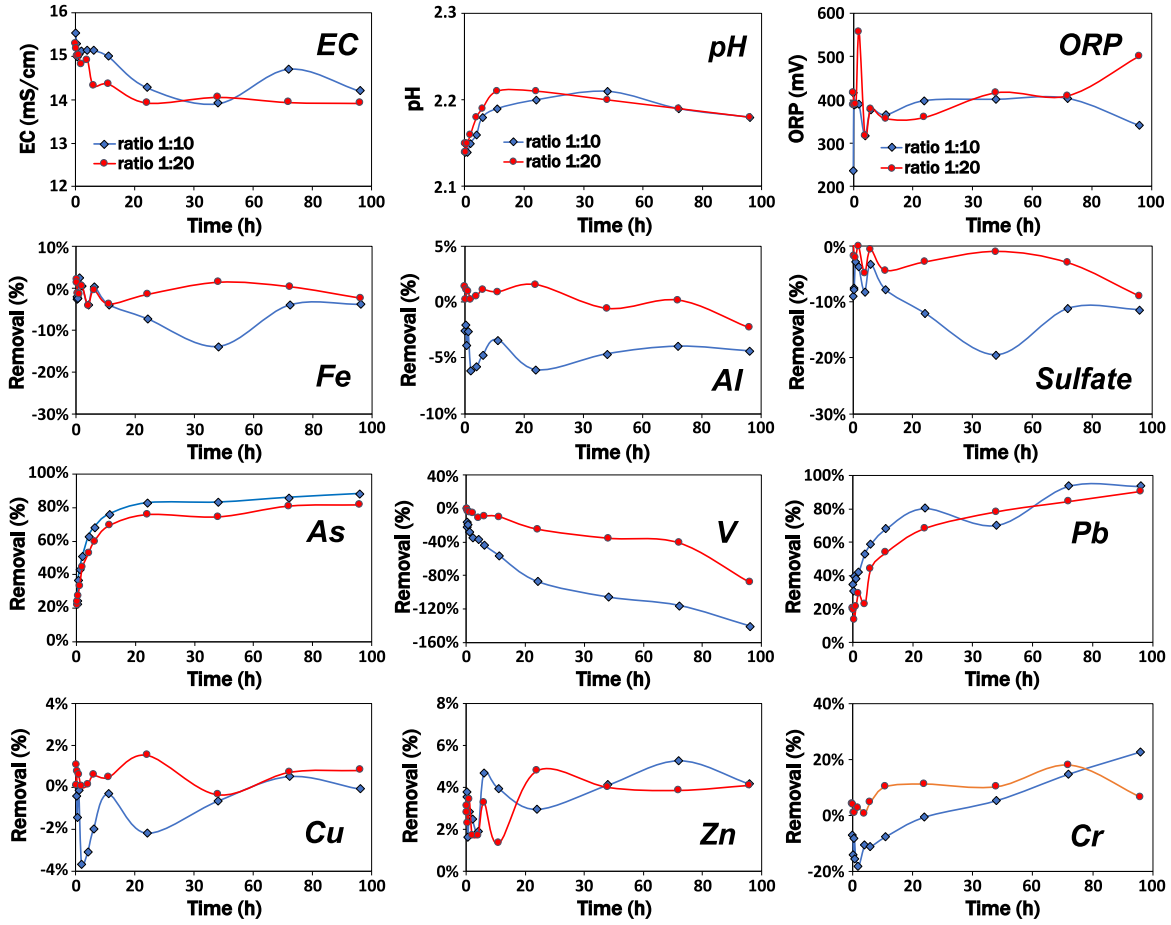

Fig. 1. Evolution of solution pH, electrical conductivity (EC), redox potential (ORP) and removal efficiency of common AMD contaminants during the batch experiments using schwertmannite.

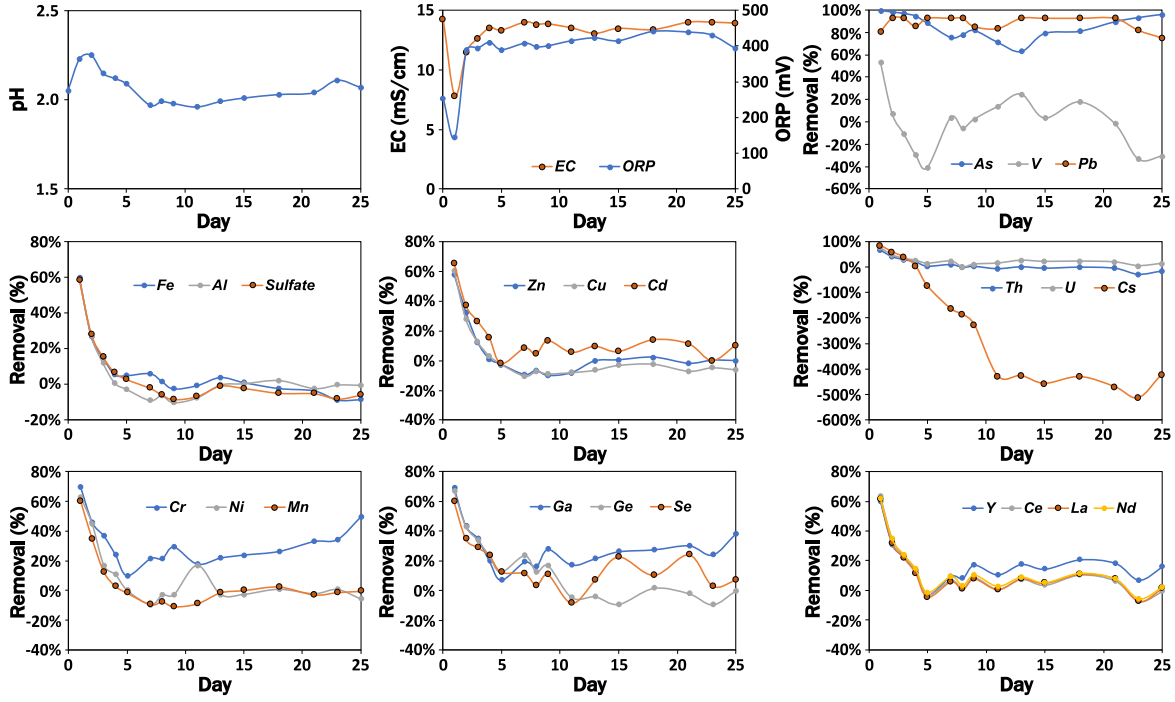

Fig. 2. Evolution of different physico-chemical parameters (i.e., pH, EC and ORP) and removal efficiency of different elements commonly found in AMD during the column experiments using schwertmannite.

(Fig. S1), especially for the ratio 1:10.

On the contrary to these elements, As and Pb followed a progressive depletion from solution, achieving removal rates of 82–88 % and 90–93 % of As and Pb, respectively (Fig. 1). In the case of V, this metalloid showed the opposite tendency, increasing its concentrations with respect the initial ones for both ratios (87 % and 140 % for 1:20 and 1:10, respectively; Fig. 1).

3.3. Column experiments

The interaction of the acidic waters with the column filled with schwertmannite led to a slight increase in pH values (from 2.04 to 2.25; day 2; Fig. 2), which coincides with a significant decrease of EC and ORP values (from 14.3 to 7.9 mS/cm and 250 to 144 mV after 24 h, respectively). However, these values recovered thereafter and remained quite stable after the end of the experiment (pH 2.07, EC 13.9 mS/cm; Fig. 2). Unlike the batch experiments, where a sharp increase of Fe, sulfate and Al concentrations was observed at the beginning of the experiment, column experiments recorded a sharp removal of these compounds, with maximum removal rates of around 60 %, decreasing progressively thereafter until achieving increases in concentrations ranging from 1 % to 8 % at the end of the experiment. The same tendency is observed for other elements such as Zn, Cu, Cd, Cr, Ni, Mn, Ga, Ge, Se or REE (Fig. 2). However, a net removal is observed for Cr (10–49 %), Ga (7–38 %), Se (3–24 %), Cd (8–11 %), and Y (3–20 %) (Fig. 2).

In the case of As and Pb, removal rates ranged from 63 % to 99 % and 74–92 %, respectively (Fig. 2), during the entire experiment, with higher values for As at the beginning and at the end. A lower removal rate was observed for V at the beginning of the experiment (53 %), decreasing progressively until achieving a 40 % of release to solution at day 5 (Fig. 2). Afterwards, this tendency changes and an accumulation of V is observed in the column (up to 24 %; Fig. 2), decreasing once again at the end of the experiment. Regarding U, Th and Cs, these elements suffered a sharp removal rate at the beginning of the experiment (66 %–83 %), decreasing progressively although following a different tendency. In the case of U, a net removal was maintained during the whole experiment, while Th was mainly retained in the column until the day 9, being released afterwards (28 % with respect initial concentration). This process was more marked for Cs, with increases of up to 500 % with respect the initial concentration (Fig. 2).

4. Discussion

4.1. Geochemical reactions controlling metal/loid removal

Fig. 3 displays the saturation indices (SI) of samples during the batch experiments. As can be seen, samples exhibit schwertmannite undersaturation for both ratios, and oversaturation with respect jarosite ($KFe(SO_4)_2(OH)_6$). Both mineral phases tend to control not only Fe solubility in acidic systems but also other metals such as Cu, Zn, Cd, or Pb by coprecipitation (Nordstrom and Alpers, 1999). Thus, the dissolution of schwertmannite may explain the initial increase of sulfate and metals (Fe, Al, Cu, or Cr; Fig. 1) concentrations observed during the batch experiments, while the precipitation of jarosite could retain some of these metals. The decrease in the concentration of sulfate, especially in the column experiment, could be also attributed to jarosite and even gypsum

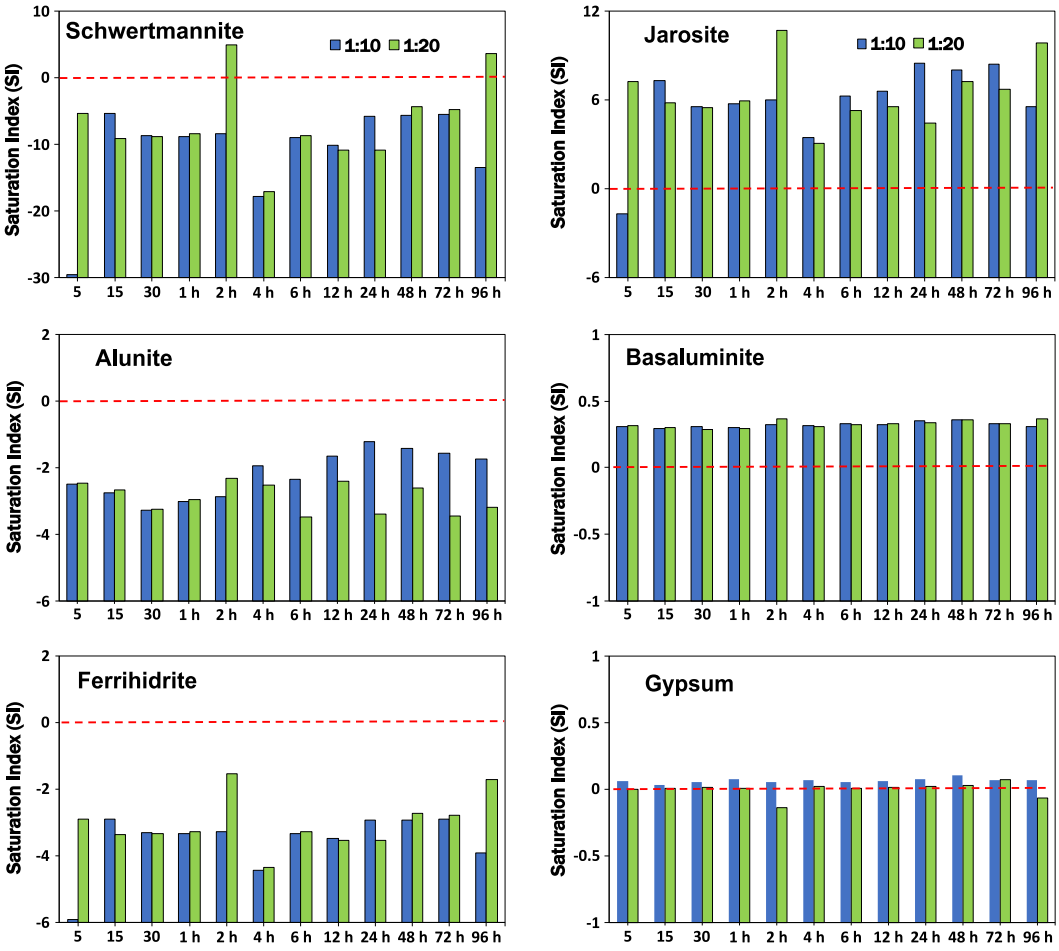

Fig. 3. Saturation indices (SI) of batch outflows with respect to main sulfate, Fe and Al minerals commonly found in AMD environments. Discontinuous red line show saturation of water with respect the mineral. SI values > 0 would indicate mineral precipitation while values < 0 would indicate dissolution (if present).

($CaSO_4$•$2H_2O$) precipitation. Gypsum seems to be in equilibrium in all samples during the experiment (Fig. 3). The acidic conditions recorded during the experiment may also preclude the precipitation of other common minerals in AMD systems, such as ferrihydrite (Fe_2O_3•$0.5H_2O$), alunite ($KAl_3(SO_4)_2(OH)_6$) or basaluminite ($Al_4(SO_4)_{1.2}(OH)_{9.6}$•$9–10H_2O$), expected to precipitate at higher pH values. In this latter case, the mobility of Al seems to be controlled by the dissolution of schwertmannite and precipitation of jarosite, since Al tends to replace Fe in both minerals (e.g., Carrero et al., 2022; Grigg et al., 2024). Thus, the predominance of one process over another may regulate the concentration of Al during the batch experiment.

Sorption processes onto these minerals (i.e., schwertmannite and jarosite) play a key role in trace metal mobility in AMD systems (e.g., Accornero et al., 2005; Antelo et al., 2013; Asta et al., 2009). The surface of both minerals is positively charged at acidic conditions; therefore, these minerals may preferentially retain negatively charged species during the experiments. Fig. 4 and S2 show the speciation of some trace elements provided by PHREEQC code during the batch experiments. As can be seen, divalent metals such as Cu, Zn, Mn, Co, or Ni are mainly found as free species (i.e., Cu^{2+}, Zn^{2+}, etc.) and non-charged sulfate complexes (i.e., $CuSO_4$, $ZnSO_4$, etc.), therefore, these metals tend not to undergo sorption processes onto Fe minerals with positively charged surfaces, but probably potential coprecipitation into jarosite. In the case of Al, due to its presence in schwertmannite replacing Fe^{3+} in its structure, the Al released during schwertmannite dissolution would not be retained back by sorption onto this mineral, except during the S:L ratio 1:20, when a significant proportion of negatively-charged sulfate complexes (i.e., $Al(SO_4)_2^-$; Fig. 4) was observed.

This process may be critical for As removal during the experiment, since As was mainly found as oxyanion ($H_2AsO_4^-$ > 50 %). This explains the higher performance achieved for As in both ratios compared to some base metals such as Cu, Zn, or Cd. Other metals which exhibited negatively charged species are U, Th, Se, Pb or REE. For example, the formation of negatively charged sulfate complexes of U and Th ($UO_2(SO_4)_2^{2-}$; 40–50 %, $Th(SO_4)_3^{2-}$; 30–40 %, Fig. 4) could suggest the removal of both elements during the experiment, however, their dissolved concentration increased (Fig. S1). It is hypothesized that strong competition processes for sorption sites with As, may have favored the release of these elements from schwertmannite and the incorporation of As into this Fe mineral. Cesium and Cr were mainly found as free species (i.e., Cs^+ Cr^{3+}; Fig. S2), therefore their mobility may be controlled by coprecipitation/dissolution processes of Fe minerals, and discarding the role of sorption processes. Vanadium is another element commonly affected by sorption processes onto Fe minerals due to its affinity to form negatively charged species. However, during the batch experiments V formed mainly non-charged sulfate complexes and positively charged species (i.e., $VOSO_4$ and VO^{2+}; Fig. 4), which may explain the net release of this element during the batch experiment.

Like in batch experiments, the precipitation of jarosite and dissolution of schwertmannite (Fig. 5) in the column seem to control Fe solubility during the experiment, while the mobility of the rest of elements would be controlled by their incorporation onto these minerals according to their speciation (Fig. 5 and Fig S3). However, coinciding the initial decrease in Fe concentration, jarosite precipitation may be predominant. This sharp decrease in Fe, together with other elements (Fig. 2), could be attributed to the interaction of the AMD solution with calcareous sands used as drain layer in the columns. These sands should be inert since their role is to improve hydraulic conductivity in columns,

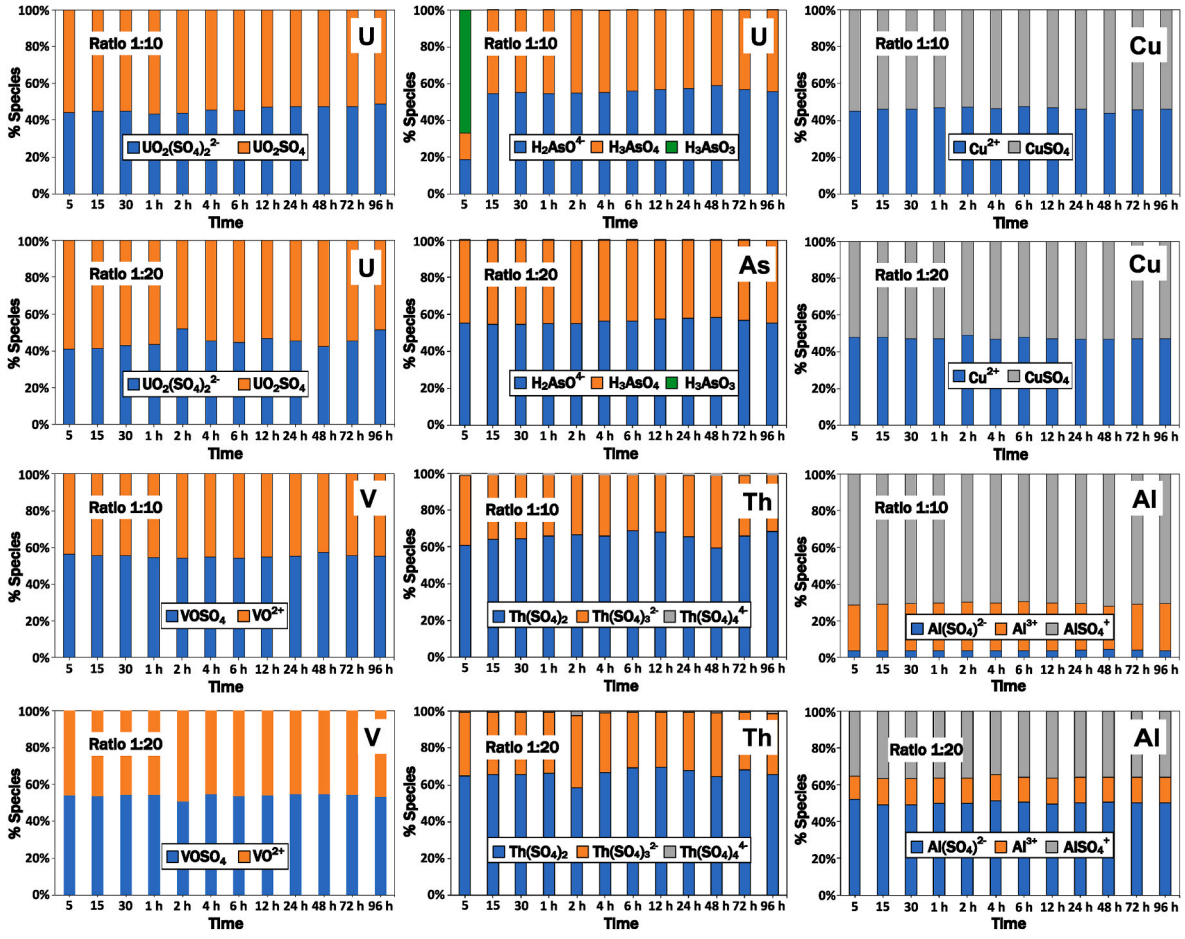

Fig. 4. Speciation modelling provided by PHREEQC code for some trace metal/loids analyzed during the batch experiments.

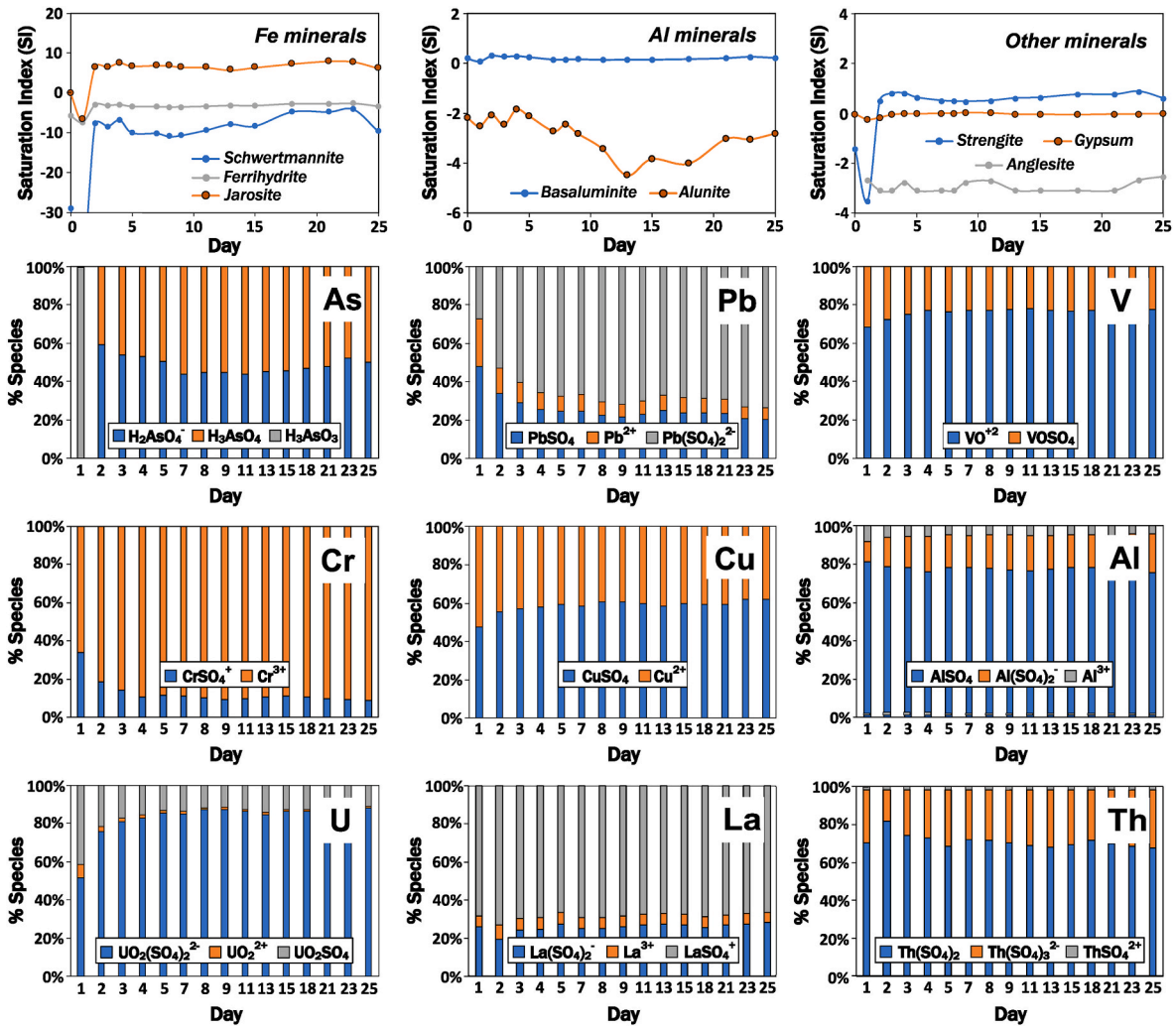

Fig. 5. Speciation and saturation indices (SI) provided by PHREEQC code for selected trace metal/loids and minerals during the column experiments.

but the dissolution of carbonates may have led to increasing Fe precipitation. Although this may have influenced the observed Fe behavior at the beginning of the experiment, and that including a blank control column (with no reactive adsorbent) or using an inert medium such as glass beads would have allowed for clearer attribution of chemical changes to the adsorbent material alone, this limitation did not compromise the overall trends observed in the column experiment, which will be discussed. In this sense, the precipitation of jarosite may dominate during the first 3 days and afterwards the dissolution of schwertmannite may balance jarosite precipitation. According to PHREEQC, strengite ($FePO_4{\cdot}2H_2O$) could also precipitate during the experiment (Fig. 5), however, it may play a minor role in Fe solubility since the concentration of P in the AMD used is low (Table 2). The model also predicts the precipitation of basaluminite, an Al hydroxisulfate which typically controls Al solubility in acidic systems at pH 4.5–5.0 (Lozano et al., 2018; Schoepfer and Burton, 2021), however the low pH values observed 2.0–2.3 together with FESEM images (Figs. S4-S10), which evidences the association of Al to schwertmannite, rule out the precipitation of this mineral during the experiment. Like in batch experiments, sorption processes onto Fe minerals seem to be the main mechanism of metal/loid removal, mainly associated to the formation of negatively charged species (e.g., $H_2AsO_4^-$, $Pb(SO_4)_2^{2-}$, $UO_2(SO_4)_2^{2-}$, and $Th(SO_4)_3^{2-}$; Fig. 5). Other elements exhibiting positively charged and neutral species (Cu, Zn, Cd, etc; Fig. 5 and Fig. S3) were not significantly affected by these processes and their incorporation into the solid phase may occur through coprecipitation processes onto precipitating jarosite, however these processes may be of minor importance considering the low removal values observed after day 3 (Fig. 3). An exception to this general tendency is observed for Cr, which speciation is dominated by positively charged species (Fig. 5). However, it has been reported that Cr^{3+} can be incorporated to secondary Fe minerals as impurities (e.g., Accornero et al., 2005).

4.2. Environmental and technical implications

Cao et al. (2021) attributed the removal of As by schwertmannite to SO_4^{2-} substitution by As(V) at acidic conditions (pH 2) due to the formation of oxyanions. The exchange of SO_4^{2-} by a certain oxyanion seems to be mainly controlled by its size and coordination (Schoepfer and Burton, 2021). In the case of divalent anions such as CrO_4^{2-} or $Pb(SO_4)_2^{2-}$ a complete exchange with SO_4^{2-} may take place in the schwertmannite structure, while other trivalent anions like AsO_4^{3-} may need some remaining structural SO_4^{2-} for mineral stability (Antelo et al., 2012). This incorporation of As(V) causes a significant release of SO_4^{2-} from schwertmannite, without major degradation of the schwertmannite structure (Burton et al., 2009). Fig. 6 shows the kinetic models of adsorption of As and Pb onto schwertmannite. A power function model was selected because it provided a better empirical fit to our experimental data over the entire time range, particularly at early stages of adsorption, where many classical models such as the pseudo-first-order (PFO) or pseudo-second-order (PSO) sometimes show deviation (Fig. S11). As can be seen, an exponential increase in sorption capacity is

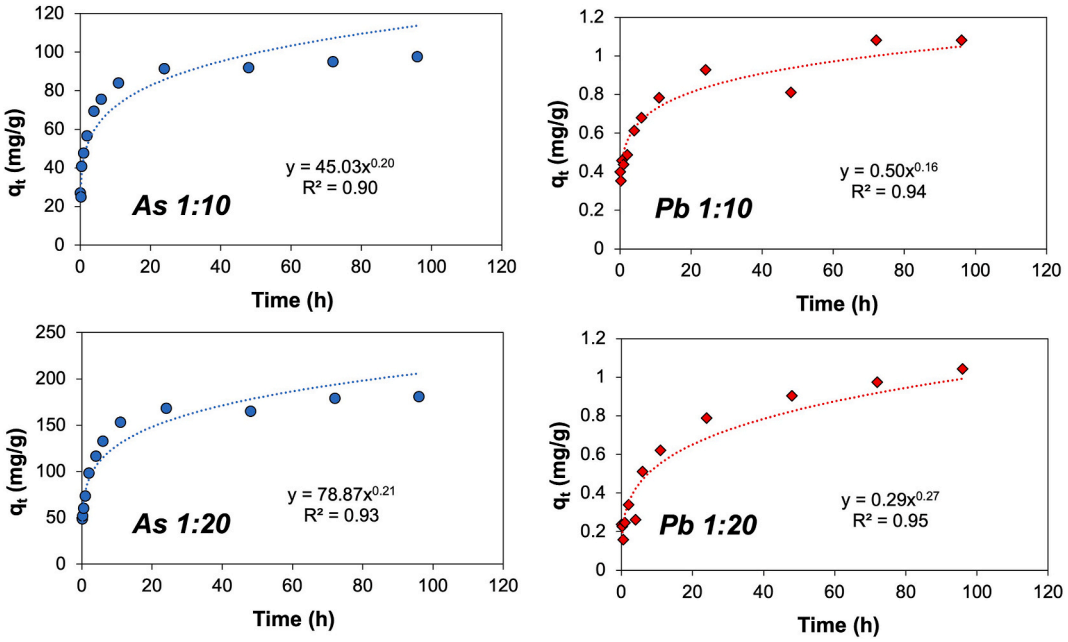

Fig. 6. Kinetic models of adsorption for As and Pb on schwertmannite during batch experiments using different S:L ratios (1:10 and 1:20). q_t: sorption (in mg/g) at a certain time t.

observed, with values of 84 and 153 mg/g of As (t = 12h) for S:L ratios 1:10 and 1:20, respectively. Then, the As sorption capacity is attenuated, reaching maximum values of 97 and 181 mg/g of As at the end of the experiment (t = 96 h). In the case of Pb, the sorption capacity is noticeably lower compared to that observed for As. An increase in sorption capacity values is observed, with values of 0.8 and 0.9 mg/g of Pb at 24 h for S:L ratios 1:10 and 1:20, respectively, decreasing the tendency afterwards (1.0 and 1.1 mg/g of Pb at the end of the experiment). Unlike in the case of As, no significant differences were found using both ratios.

These values can be compared with others reported in literature using the same or different waste materials. Xiong et al. (2023) reported maximum adsorption capacities of 102 mg/g of As in synthetized schwertmannite using lab solutions of 20 mg/L and a solid ratio of 1 g/L. Different technological solutions have been also proposed to remove As from industrial and mine waters. For example, Gupta et al. (2012) explored the potential removal of As with nanostructured cerium incorporated manganese oxide. These authors reported optimal values of 38 mg/g at a pH range of 7–8. Lima et al. (2022) investigated the use of composts and biochars derived from the organic fraction of municipal solid wastes and obtained maximum As sorption capacities ranging from 0.07 to 170 mg/g using solutions of 0.5–100 mg/L of As. Ocinski and Mazur (2020) achieved adsorption capacities for As of up to 83 mg/g using hybrid polymer obtained by entrapment of Fe-Mn waste oxides from water deironing into a chitosan matrix. Values reported using low-cost natural waste materials such as eggshells, chestnut shells or tea wastes were even lower, not exceeding maximum sorption capacities of 9 mg/kg (Shakoor et al., 2016). It is therefore remarkable the sorption capacity of natural schwertmannite investigated in this study compared to synthetics. In this sense, previous research suggests an increasing As retention by schwertmannite by metal coprecipitation (Antelo et al., 2013).

According to the good performance of schwertmannite removing trace metals such as As and Pb, this waste material generated in AMD systems could be used as a natural filter at the entrance of AMD treatment plants. Thus, the pin cushion morphology characteristic of this mineral provides enough permeability to allow the water to infiltrate through this natural filter and guaranteeing a long-lasting performance of this system. Once the schwertmannite-based filter loses its sorption capacity, this material could be safely disposed of in landfill, prior evaluation of its leaching potential (Macías et al., 2012). Nevertheless, future studies should also address the environmental impact and proper disposal of spent adsorbents. This includes evaluating their long-term stability, ability to be regenerated, leaching characteristics, and the risk of causing secondary pollution, all of which are essential for the sustainable application of these materials in mining and industrial settings.

5. Conclusions

This work assesses the suitability of using natural schwertmannite to treat highly acidic and metal-rich effluents (pH 2.0, 6664 mg/L of Fe, 910 mg/L of Al, 794 mg/L of Zn, 196 mg/L of Cu, 12.5 mg/L of As or 0.17 mg/L of Pb) through batch and column experiments. During batch experiments, the interaction of acidic waters with schwertmannite led to increased concentrations of sulfate (19 %), Fe (14 %), and Al (6 %), particularly at a 1:10 ratio, probably due to schwertmannite dissolution. Other elements such as Cr, Cu, Ni, Cd, Se, U, Th, and REE, followed the same pattern, especially at the 1:10 ratio, although Cr was subsequently removed from solution (22 %), like in the case of Zn (1.3–5.5 %). However, the most striking result is the successful removal of As and Pb (82–88 % and 90–93 %, respectively). The column experiment also obtained high removal rates for As and Pb (63–99 % and 74–92 %, respectively). Unlike in the batch experiment, interaction with schwertmannite led to a significant drop in EC and metal/loidss concentration (up to 60 %) within 24 h, attributed to the dissolution of carbonates from sandy material used in the column drain. Afterwards, these values later stabilized, ending the experiment with a slight concentration increase (1–8 %) for most elements, though Cr, Ga, Se, Cd, U and Y showed net removal (10–49 %, 7–38 %, 3–24 %, 8–11 %, 1–15 % and 3–20 %, respectively).

The precipitation of jarosite and dissolution of schwertmannite in the column seem to control Fe solubility during the experiment. The mobility of the rest of elements would be controlled by their incorporation onto these minerals by sorption and/or coprecipitation according to their speciation. In this way, elements exhibiting negatively charged species would be preferentially removed by sorption due to the positively charged surface of schwertmannite upon acidic conditions, while

others could coprecipitate with newly formed jarosite.

This study reported maximum sorption values of 97–181 mg/g of As and 0.8–0.9 mg/g of Pb. The adsorption capacity of natural schwertmannite in this study is notable compared to synthetic and other materials (e.g., synthetic schwertmannite, nanostructured cerium-manganese oxide, composts, biochars, Fe-Mn polymers or low-cost natural materials like eggshells and tea waste). Due to its effectiveness in removing trace metals like As and Pb, schwertmannite from AMD systems could serve as a natural filter at AMD treatment plant inlets. Its pin-cushion morphology ensures water permeability and long-lasting performance. Once saturated, the filter material could be safely disposed of in a landfill after assessing its leaching potential. The use of this waste material in AMD treatment plants worldwide could help to improve their cost-effectiveness while improving their environmental performance. However, future research should also focus on the environmental fate and safe disposal of saturated adsorbents, including long-term stability, regeneration capacity, leaching behavior and potential secondary contamination risks, to ensure sustainable use of these materials in mining and industrial applications.

CRediT authorship contribution statement

Carlos R. Cánovas: Writing – original draft, Project administration, Investigation, Formal analysis, Conceptualization. **Maira Castellanos:** Writing – review & editing, Visualization, Methodology, Formal analysis, Data curation. **Rafael Pérez-López:** Writing – review & editing, Supervision, Investigation, Funding acquisition. **Ricardo Millán-Becerro:** Writing – review & editing, Methodology, Formal analysis, Data curation. **Alberto Molinero-García:** Writing – review & editing, Methodology, Formal analysis, Conceptualization. **Manuel Olías:** Writing – review & editing, Supervision, Investigation, Conceptualization. **José Miguel Nieto:** Writing – review & editing, Project administration, Investigation, Conceptualization. **María Dolores Basallote:** Writing – review & editing, Supervision, Methodology, Funding acquisition, Conceptualization.

Declaration of competing interest

The authors declare that they have no known competing financial interests or personal relationships that could have appeared to influence the work reported in this paper.

Acknowledgements

This work was supported by the research projects ARCHENICAL and ARCHENICAL 2.0 funded by and the ATLANTIC COPPER Cátedra. M.D. Basallote thanks the Regional Government of Andalusia for the EMERGIA grant (EMC21_00363) and MCIN for the RYC2022-035326-I grant funded by MCIN/AEI/10.13039/501100011033AEI/10.13039/501100011033 and FSE+. C.R Cánovas thanks the Spanish Ministry of Science and Innovation for the Postdoctoral Fellowship granted under application reference RYC2019-027949-I funded by MCIN/AEI/10.13039/501100011033. R. Millán-Becerro also thanks the Spanish Ministry of Science, Innovation and Universities for the Juan de la Cierva Postdoctoral Fellowship (JDC2023-052111-I) supported by MCIU/AEI/10.13039/501100011033 and FSE+. Alberto Molinero-García also acknowledges Juan de la Cierva Postdoctoral Fellowship (JDC2022–049235-I) supported by MICIU/AEI/10.13039/501100011033 and the European UnionNext Generation EU/PRTR. Funding for open access charge: Universidad de Huelva/CBUA.

Appendix A. Supplementary data

Supplementary data related to this article can be found at https://doi.org/10.1016/j.jenvman.2025.127287.

Data availability

Data will be made available on request.

References

Accornero, M., Marini, L., Ottonello, G., Vetuschi Zuccolini, M., 2005. The fate of major constituents and chromium and other trace elements when acid waters from the derelict Libiola mine (Italy) are mixed with stream waters. Appl. Geochem. 20, 1368–1390. https://doi.org/10.1016/j.apgeochem.2005.03.001.

Akcil, A., Koldas, S., 2006. Acid Mine Drainage (AMD): causes, treatment and case studies. J. Clean. Prod. 14, 1139–1145. https://doi.org/10.1016/j.jclepro.2004.09.006.

Antelo, J., Fiol, S., Gondar, D., López, R., Arce, F., 2012. Comparison of arsenate, chromate and molybdate binding on schwertmannite: surface adsorption vs anion-exchange. J. Colloid Interface Sci. 386, 338–343. https://doi.org/10.1016/j.jcis.2012.07.008.

Antelo, J., Fiol, S., Gondar, D., Pérez, C., López, R., Arce, F., 2013. Cu(II) incorporation to schwertmannite: effect on stability and reactivity under AMD conditions. Geochem. Cosmochim. Acta. 119, 149–163. https://doi.org/10.1016/j.gca.2013.05.029.

Asta, M.P., Cama, J., Martínez, M., Giménez, J., 2009. Arsenic removal by goethite and jarosite in acidic conditions and its environmental implications. J. Hazard. Mater. 171, 965–972. https://doi.org/10.1016/j.jhazmat.2009.06.097.

Bigham, J.M., Schwertmann, U., Traina, S.J., Winland, R.L., Wolf, M., 1996. Schwertmannite and the chemical modeling of iron in acid sulfate waters. Geochim. Cosmochim. 60, 2111–2121. https://doi.org/10.1016/0016-7037(96)00091-9.

Burton, E.D., Bush, R.T., Johnston, S.G., Watling, K.M., Hocking, R.K., Sullivan, L.A., Parker, G.K., 2009. Sorption of arsenic(V) and arsenic(III) to schwertmannite. Environ. Sci. Technol. 43, 9202–9207. https://doi.org/10.1021/es902461x.

Cai, J.B., 2015. Research on the treatment method of acid mine water in coal mine. Guangdong Technol 24 (18), 43–50.

Cánovas, C.R., Macías, F., Olías, M., 2018. Hydrogeochemical behavior of an anthropogenic mine aquifer: Implications for potential remediation measures. Sci. Total Environ. 636, 85–93. https://doi.org/10.1016/j.scitotenv.2018.04.270.

Cao, Q., Chen, C., Li, K., Sun, T., Shen, Z., Jia, J., 2021. Arsenic(V) removal behavior of schwertmannite synthesized by $KMnO_4$ rapid oxidation with high adsorption capacity and Fe utilization. Chemosphere. 264, 128398. https://doi.org/10.1016/j.chemosphere.2020.128398.

Carrero, S., Fernandez-Martinez, A., Perez-Lopez, R., Cama, J., Dejoie, C., Nieto, J.M., 2022. Effects of aluminum incorporation on the schwertmannite structure and surface properties. Environ. Sci. Process Impacts 24, 1383–1391. https://doi.org/10.1039/D2EM00029F.

Chen, L., Zhou, M., Wang, J., Zhang, Z., Duan, C., Wang, X., Zhao, S., Bai, X., Li, Z., Li, Z., Fang, L., 2022. A global meta-analysis of heavy metal(loid)s pollution in soils near copper mines: evaluation of pollution level and probabilistic health risks. Sci. Total Environ. 835, 155441. https://doi.org/10.1016/j.scitotenv.2022.155441.

Ficklin, W.H., Plumlee, G.S., Smith, K.S., McHugh, J.B., 1992. Geochemical classification of mine drainages and natural drainages in mineralized areas. In: Proceedings of the 7th International Symposium on Water Rock Interaction, pp. 381–384. Park City, Utah.

Grigg, A.R.C., Notini, L., Kaegi, R., Thomas Arrigo, L.K., Kretzschmar, R., 2024. Aluminium substitution affects jarosite transformation to iron oxyhydroxides in the presence of aqueous Fe(II). Geochem. Cosmochim. Acta 374 (2024), 72–84. https://doi.org/10.1016/j.gca.2024.04.008.

He, X.W., Zhang, X.H., Li, F.Q., Zhang, C.H., 2018. Comprehensive utilization system and technological innovation of water resources in coal mines. Coal Sci. Technol. 46 (9), 4–11.

Hudson-Edwards, K., 2016. Tackling mine wastes. Science 352 (6283), 288–290.

Johnson, D.B., Hallberg, K.B., 2005. Acid mine drainage remediation options: a review. Sci. Total Environ. 338, 3–14. https://doi.org/10.1016/j.scitotenv.2004.09.002.

Lima, J.Z., Ferreira da Silva, E., Patinha, C., Duraes, N., Vieira, E.M., Rodrigues, V.G.S., 2022. Sorption of arsenic by composts and biochars derived from the organic fraction of municipal solid wastes: kinetic, isotherm and oral bioaccessibility study. Environ. Res. 204, 111988. https://doi.org/10.1016/j.envres.2021.111988.

Lozano, A., Fernández-Martínez, A., Ayora, C., Poulain, A., 2018. Local structure and ageing of basaluminite at different pH values and sulphate concentrations. Chem. Geol. 496, 25–33. https://doi.org/10.1016/j.chemgeo.2018.08.002.

Macías, F., Caraballo, M.A., Nieto, J.M., 2012. Environmental assessment and management of metal-rich wastes generated in acid mine drainage passive remediation systems. J. Hazard. Mater. 229–230, 107–114. https://doi.org/10.1016/j.jhazmat.2012.05.080.

Naidu, G., Ryu, S., Thiruvenkatachari, R., Choi, Y., Jeong, S., Vigneswaran, S., 2019. A critical review on remediation, reuse, and resource recovery from acid mine drainage. Environ. Pollut. 247, 1110–1124. https://doi.org/10.1016/j.envpol.2019.01.085.

Nieto, J.M., Sarmiento, A.M., Canovas, C.R., Olias, M., Ayora, C., 2013. Acid mine drainage in the Iberian Pyrite Belt: 1. Hydrochemical characteristics and pollutant load of the Tinto and Odiel rivers. Environ. Sci. Pollut. Res. 20, 7509–7519. https://doi.org/10.1007/s11356-013-1634-9.

Nordstrom, D.K., Alpers, C.N., 1999. Geochemistry of acid mine waters. The environmental geochemistry of mine waters, 6A. Rev. Econ. Geol. 133–160.

Nordstrom, D.K., Wilde, F.D., 1998. Reduction–oxidation potential (electrode method). National fieldmanual for the collection of water quality Ddata. U.S. geological

survey techniques of Water-resources investigations, 9. U.S. Geological Survey, Reston, Va, p. 20 chapter 6.5.

Ocinski, D., Mazur, P., 2020. Highly efficient arsenic sorbent based on residual from water deironing–Sorption mechanisms and column studies. J. Hazard. Mater. 382, 121062. https://doi.org/10.1016/j.jhazmat.2019.121062.

Orden, S., Macías, F., Cánovas, C.R., Nieto, J.M., Pérez-López, R., Ayora, C., 2021. Eco-sustainable passive treatment for mine waters: full-scale and long-term demonstration. J. Environ. Manage. 280, 111699. https://doi.org/10.1016/j.jenvman.2020.111699.

Parkhurst, D.L., Appelo, C.A.J., 2013. Description of input and examples for PHREEQC version 3—A computer program for speciation, batch-reaction, one-dimensional transport, and inverse geochemical calculations, 6. U.S. Geological Survey Techniques and Methods, p. 497. https://doi.org/10.3133/tm6A43 chap. A43.

Sánchez-España, J., Yusta, I., Gray, J., Burgos, W.D., 2016. Geochemistry of dissolved aluminium at low pH: extent and significance of Al-Fe(III) coprecipitation below pH 4.0. Geochem. Cosmochim. Acta 175, 128–149. https://doi.org/10.1016/j.gca.2015.10.035.

Schoepfer, V.A., Burton, E.D., 2021. Schwertmannite: a review of its occurrence, formation, structure, stability and interactions with oxyanions. Earth Sci. Rev. 221, 103811. https://doi.org/10.1016/j.earscirev.2021.103811.

Shakoor, M.B., Niazi, N.K., Bibi, I., Murtaza, G., Kunhikrishnan, A., Seshadri, B., Shahid, M., Ali, S., Bolan, N.S., Ok, Y.S., Abid, M., Ali, F., 2016. Remediation of arsenic-contaminated water using agricultural wastes as biosorbents. Crit. Rev. Environ. Sci. Technol. 46 (5), 467–499. https://doi.org/10.1080/10643389.2015.1109910.

Xiong, H.X., Hu, D., Shi, K., Zhu, S.B., Xu, Y.Q., 2023. Adsorptive removal of arsenic ions from contaminated water using low-cost schwertmannites and akaganeites. Mater. Chem. Phys. 297, 127411. https://doi.org/10.1016/j.matchemphys.2023.127411.

Ziemkiewicz, P., Skousen, J., Simmons, J., 2003. Long-term performance of passive acid mine drainage treatment systems. Mine Water Environ. 22, 18–129. https://doi.org/10.1007/s10230-003-0012-0.